

Soft-X-Ray Vortex Beam Detected by Inline Holography

Yuta Ishii^{1,*}, Kohei Yamamoto², Yuichi Yokoyama³, Masaichiro Mizumaki³, Hironori Nakao⁴, Taka-hisa Arima⁵, and Yuichi Yamasaki^{4,6,5,7}

¹*Department of Physics, Tohoku University, Sendai 980-8578, Japan*

²*Division of Electronic Structure, Department of Materials Molecular Science, Institute for Molecular Science, Okazaki 444-8585, Japan*


³*Japan Synchrotron Radiation Research Institute (JASRI/SPring-8), Sayo 679-5198, Japan*

⁴*Photon Factory, Institute of Materials Structure Science, High Energy Accelerator Research Organization, Tsukuba 305-0801, Japan*

⁵*RIKEN Center for Emergent Matter Science (CEMS), Wako 351-0198, Japan*

⁶*Research and Services Division of Materials Data and Integrated System (MaDIS), National Institute for Materials Science (NIMS), Tsukuba 305-0047, Japan*

⁷*PRESTO, Japan Science and Technology Agency (JST), Kawaguchi 332-0012, Japan*

 (Received 30 June 2020; revised 22 November 2020; accepted 24 November 2020; published 24 December 2020)

We demonstrate inline holography with a soft-x-ray vortex beam having an orbital angular momentum. A hologram is recorded as an interference pattern between a Bragg-diffracted wave from a fork grating and a divergent wave generated by a Fresnel zone plate. The images obtained exhibit fork-shaped interference fringes, which confirm the formation of a vortex beam. By analyzing the interference images, we successfully obtain a spiral phase distribution with a topological charge $\ell = \pm 1$. The results demonstrate that the inline-holography technique may be an effective probe for the characterization of topological defects in magnetic textures.

DOI: [10.1103/PhysRevApplied.14.064069](https://doi.org/10.1103/PhysRevApplied.14.064069)

I. INTRODUCTION

A vortex wave function $\psi = \exp(i\ell\phi)$, where ϕ is the azimuthal angle in cylindrical coordinates, is an eigenstate of the orbital-angular-momentum (OAM) operator $\hat{L}_z = -i\hbar \partial/\partial\phi$ with an eigenvalue $\ell\hbar$. Therefore, a spiraling wavefront of a particle provides an OAM around the propagation axis, and a vortex beam is characterized by a topological charge ℓ , defined as

$$\ell = \frac{1}{2\pi} \oint_C \nabla\theta(\mathbf{r}) \cdot d\mathbf{r}, \quad (1)$$

where θ represents the phase distribution, and C represents a closed loop surrounding the propagation axis. The demonstration of a vortex beam with visible light generated in free space [1] has attracted significant interest in diverse research fields [2], including superresolution microscopy [3], optical tweezers [4], and quantum information processes [5].

The generation of soft-x-ray vortices from undulators [6], spiral zone plates [7], and diffractive optics [8] has also been investigated. Soft x rays tuned to the absorption energy of an element are widely used to investigate the

magnetic state of materials containing a $3d$ or $4f$ transition element, owing to their high sensitivity to the spin density of unoccupied states. Thus, soft-x-ray diffraction with coherent wavefronts is a suitable technique for real-space observation of magnetic textures [9–11].

Meanwhile, it has been reported in the case of coherent hard-x-ray imaging of a silicon single crystal that vortex beams can be produced by dislocation singularities in the crystal, which can be regarded as topological defects [12]. Correspondingly, soft x rays could be converted to a vortex beam via a topological defect in a magnetic texture, such as a dislocation in a magnetic skyrmion lattice or a magnetic Bloch point in a skyrmion or helical lattice [13–16]. In particular, characterizing dislocations in skyrmion domains would lead to great understanding of the topological stabilization of skyrmions. Furthermore, the dynamics of such topological defects have been the focus of intensive research because of the possibility of practical applications in magnetic memory devices [15]. Hence, characterizing and visualizing these defects are vital for research in topological magnetism, and soft-x-ray imaging techniques probing generated vortex beams may be effective imaging probes for them. To this end, clarifying the phase distribution and the phase singularities of vortex beams is crucial.

*yuta.ishii.c2@tohoku.ac.jp

However, it is impossible to directly obtain information about the phase of soft x rays by observing the intensity. For visible light, an interference measurement can be performed to visualize the phase distribution of a vortex beam using optical elements such as beam splitters and mirrors [17,18]. Meanwhile, the lack of optical elements for soft x rays, such as suitable mirrors, renders it difficult to perform an interference experiment. Another interference method is inline (Gabor) holography, in which a reference wave and a diffracted wave scattered by an object share the same optical axis. The usefulness of this technique for obtaining spiral phase distributions in electron vortex beams has been demonstrated [19,20]. Hence, in the present study, we focus on the observation of phase information about soft-x-ray vortices generated by a diffractive optical element via coherent soft-x-ray inline holography.

A vortex beam in a Laguerre-Gaussian mode [21] with a zero radial index and an integer topological charge $\ell = nb$ can be produced in the n th Bragg diffraction from a fork grating with a topological number b [22,23]. The phase distribution at the fork grating can be expressed as

$$\varphi(\rho, \phi) = b\phi + \frac{2\pi}{d}\rho \cos \phi \quad (2)$$

in cylindrical coordinates (ρ, ϕ, z) , where d is the pitch of the grating far from the center ($\rho = 0$). The binarized amplitudes corresponding to the opaque and transparent regions are

$$a(\varphi) = \begin{cases} 1, & \text{if } \text{mod}(\varphi, 2\pi) < \pi, \\ 0, & \text{otherwise,} \end{cases} \quad (3)$$

which results in the pattern shown in Fig. 1(a) for $b = 1$. This fork-shaped pattern can be regarded as a topological phase defect. Similar patterns are commonly seen in some topological magnets [13–16,24]. The transmitted field u_1 is calculated in the form of a Fourier series as

$$u_1 = u_0 a(\varphi) = u_0 \sum_{n=-\infty}^{\infty} A_n e^{-in(\pi/2)} e^{in\varphi}, \quad (4)$$

where

$$A_n = \frac{\sin(n\pi/2)}{n\pi} \quad (5)$$

and the incident field is $u_0 = u_0(\rho, \phi)$ [25]. The far-field diffraction output u_2 can be derived from the Fourier transform $\mathcal{F}[u_1]$, which results in

$$u_2(f_x, f_y) \propto \sum_{n=-\infty}^{\infty} u_0 e^{in[b\phi_{kn} + (\pi/2)(b-1)]} A_n \mathcal{J}_{nb}(\rho_{kn}), \quad (6)$$

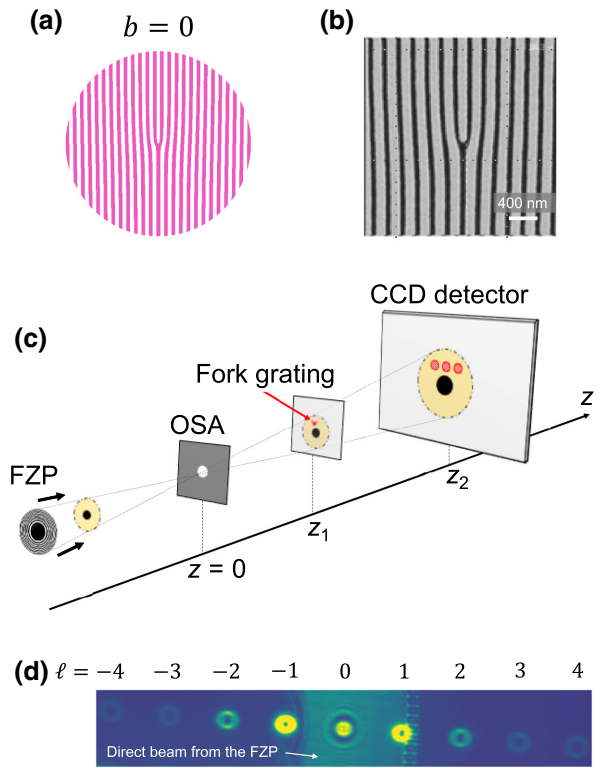


FIG. 1. (a) Schematic illustration of a fork grating with $b = 1$. (b) Scanning-electron-microscopy image of the central part of the fork grating used in this study. Ta metal (gray) is deposited on a membrane of Si_3N_4 . (c) Experimental setup for coherent soft-x-ray inline holography. Incident x rays are focused using a Fresnel zone plate (FZP). The first-order diffraction from the FZP is selected by an order-sorting aperture (OSA) placed at the focal point. The zeroth-order direct beam is stopped by center stops on the FZP and the OSA. Bragg-diffracted waves, which occur at the fork grating located downstream of the focal point, interfere with waves transmitted outside the grating. (d) Diffraction pattern from fork grating without interference, which shows diffraction up to the fourth order.

where (ρ_{kn}, ϕ_{kn}) denotes cylindrical coordinates with $(f_x, f_y) = (2\pi n/d, 0)$ as the origin. $\mathcal{J}_{nb}(\rho_{kn})$ can be calculated as

$$\mathcal{J}_{nb}(\rho_k) = \int_0^a \rho J_{nb}(\rho_k \rho) d\rho, \quad (7)$$

where $J_{nb}(x)$ is the n th Bessel function of the first kind, and the radius of the grating is a . The result indicates that the diffracted wave in the n th Bragg diffraction has an OAM with $L_z = \ell \hbar = nb \hbar$. These facts indicate that a topological phase defect in an object such as a fork-shaped pattern of the kind shown in Fig. 1(a) can produce a vortex beam with a phase singularity reflecting the topological features.

II. EXPERIMENTAL DETAILS

A soft-x-ray diffraction measurement does not provide any information about the phase factor $e^{i\ell\phi_k}$, as only the intensity $I = |u_2|^2$ is observable. Therefore, we observe the interference between the diffracted waves and divergent waves from a Fresnel zone plate, as shown in Fig. 1(c), which illustrates schematically the inline-holography setup. Soft-x-ray experiments are performed at the soft-x-ray undulator beamlines BL-13A and BL-16A at the Photon Factory, KEK, Japan. The wavelength λ of the soft x rays is tuned to 1.6 nm, which ideally results in a focal length of 1.5 mm via a FZP with outer and center beam-stopper radii of 60 and 30 μm , respectively. The higher-order diffractions from the FZP are filtered by an order-sorting-aperture with a radius of 5 μm located at the focal position of the FZP. A fork grating with $b = 1$ is made from Ta metal with a thickness of 300 nm deposited on a membrane of Si_3N_4 . Figure 1(b) shows a scanning-electron-microscopy image of the grating. The grating has a nominal 200-nm period and a radius $a = 2.5 \mu\text{m}$. The absence of patterning outside the grating enables reference waves to pass through the grating and interfere with the diffracted waves. The diffraction pattern is recorded using an in-vacuum CCD camera (Teledyne Princeton PMI2048, 2048 \times 2048 pixels, pixel size 13 μm) installed at a distance $z_2 = 220 \text{ mm}$ from the focal position.

III. RESULTS AND ANALYSIS

Figure 1(d) shows a diffraction pattern obtained from the fork grating when it is placed in the right part of the annular diffraction from the FZP. In this case, the diffraction from the grating is observed without being superimposed on the transmitted waves. Each Bragg diffraction, from the first to the fourth, exhibits a ringlike intensity distribution, which is characteristic of a vortex beam, and is expected to have an OAM $L_z = n\hbar$. Based on Eq. (5), the diffractions with $n = 2$ and 4 should vanish, provided that the grating forms an ideal square wave. The appearance of even-number-order Bragg diffractions is likely to be because the widths of the transparent and opaque regions do not match perfectly.

Figure 2(a) shows the diffraction pattern when the grating is placed $z_1 = 680 \mu\text{m}$ away from the focal point, in the upper part of the annular diffracted waves from the FZP. In this case, an interference pattern is observed because the first diffraction from the grating overlaps with the waves from the FZP. Intensity modulations along the horizontal direction are clearly visible; these cannot be observed in the absence of interference. In addition, the upper half of the diffraction pattern contains an additional stripe compared with the lower half, and a fork-shaped pattern appears at the center. Such a pattern implies the formation of a vortex beam with a phase rotating from 0 to 2π along the azimuthal-angle direction. We simulate an

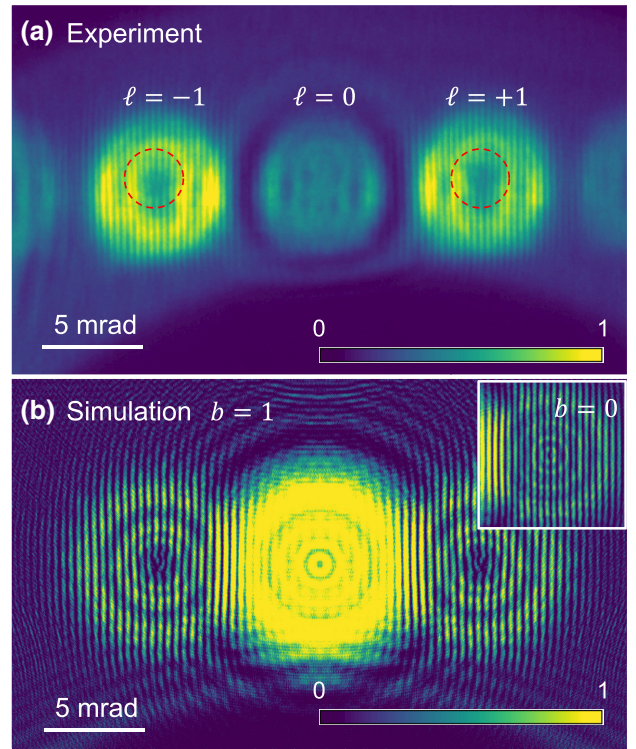


FIG. 2. (a) Experimental results for inline holography of the diffraction of a vortex beam interfering with the transmitted reference beam. The dashed circles indicate fork-shaped patterns appearing in the Bragg diffractions with $\ell = -1$ and $\ell = +1$. The length of the scale bar represents an angle of 5 mrad measured from the fork grating. (b) Simulated interference pattern from a fork grating with $b = 1$; the pattern from a rectilinear grating ($b = 0$) is shown in the inset.

interference pattern using a scaled fast-Fourier-transform method [26], assuming an ideal FZP and a fork grating with $b = 1$. Figure 2(b) shows the simulated interference pattern, which agrees reasonably well with the experimental result. Furthermore, we simulate the case for a rectilinear grating ($b = 0$), as shown in the inset of Fig. 2(b), confirming that there is no fork-shaped pattern at the center in this case.

As similar intensity patterns have been observed in visible-light and electron vortex beams [17,20], it is known that such interference patterns require a reference beam from an inclined direction. To gain further understanding of the intensity distributions shown in Figs. 2(a) and 2(b), we perform an analytical calculation assuming a divergent wave from a point light source at the focal position of the FZP. It is assumed that a point source exists at the origin, and that the grating is in the $z = z_1$ plane and the detector is in the $z = z_2$ plane in the Cartesian coordinates shown in Fig. 1(c). The direct light field u_2^d at the detector plane

(x_2, y_2, z_2) is expressed as

$$u_2^d(x_2, y_2, z_2) = \frac{u_0 e^{ikr_2}}{r_2} \sim \frac{u_0}{z_2} e^{ik\{z_2 + [(x_2^2 + y_2^2)/2z_2]\}}, \quad (8)$$

where r_2 is the distance between the detection point and the point source; furthermore, we use the paraxial approximation ($x_2^2 + y_2^2 \ll z_2^2$). The diffracted wave from the grating, $u_2^g(x_2, y_2, z_2)$, is expressed as

$$u_2^g(x_2, y_2, z_2) = -\frac{i}{\lambda} \iint_G \frac{e^{ikr}}{r} u_1(x_1, y_1) dx_1 dy_1, \quad (9)$$

where G denotes the integral within the grating region, and $r = \sqrt{(x_1' - x_2)^2 + (y_1' - y_2)^2 + (z_1 - z_2)^2}$ denotes the distance between the detection point and the position $Q = (x_1', y_1', z_1)$ on the grating where an x ray passes through. The diffraction pattern of these two waves can be calculated as

$$I(x_2, y_2) = |u_2^d|^2 + |u_2^g|^2 + u_2^d u_2^{g*} + \text{c.c.}, \quad (10)$$

where ‘‘c.c.’’ represents the complex conjugate. The interference term of the n th Bragg diffraction from a fork grating with $b = 1$ is calculated as

$$I_n^{\text{inter}} = 2C_n |\mathcal{J}'_n| \sin\{kR_2 + n\phi_{fn} + \alpha_n\}, \quad (11)$$

where $C_n = 2A_n \pi u_0^2 / \{\lambda z_1 z_2 (z_2 - z_1)\}$,

$$\mathcal{J}'_n(\rho_{fn}) = \int_0^a e^{if_0 \rho^2} \rho J_n(\rho_{fn} \rho) d\rho \equiv |\mathcal{J}'_n(\rho_{fn})| e^{i\alpha_n}, \quad (12)$$

and

$$R_2 = \frac{z_1}{2z_2(z_2 - z_1)} \left\{ \left(x_2 - \frac{z_2}{z_1} x_g \right)^2 + \left(y_2 - \frac{z_2}{z_1} y_g \right)^2 \right\}, \quad (13)$$

and where (ρ_{fn}, ϕ_{fn}) are local cylindrical coordinates with $(x_{2n}, y_{2n}) = [z_2 x_g / z_1 + 2n\pi(z_2 - z_1)/kd, z_2 y_g / z_1]$ as the origin, which corresponds to the center of the n th Bragg diffraction, and (x_g, y_g, z_1) is the center of the grating. (The details of the calculation above are included in the Appendix.) The integral in Eq. (12) is different from that in Eq. (7) in terms of the factor $e^{if_0 \rho^2}$, with $f_0 = kz_2/2z_1(z_2 - z_1)$, which originates from near-field diffraction, i.e., Fresnel diffraction [27]. Equation (11) includes a term $n\phi_{fn} = \ell\phi_{fn}$ in the sine function, which imposes spiral phase information on the observable intensity, thereby resulting in a fork-shaped pattern at the center of the diffraction. R_2 varies in the radial direction from the zero-order diffraction, and produces stripelike intensity modulations along the horizontal direction. Furthermore, $\alpha_n(\rho_{fn})$ results in

modulations in the radial direction from (x_{2n}, y_{2n}) , which are independent of the azimuthal angular direction. These features are observed in both the experimental and the simulated results.

The Fourier transform \mathcal{F} of the n th Bragg diffraction I_n is expressed as

$$\mathcal{F}[I_n(x_2, y_2)] = G_n^0(0, 0) + G_n^+(q_x, q_y) + G_n^-(q_x, -q_y), \quad (14)$$

where G_n^0 and G_n^\pm are derived from the noninterference and interference terms, respectively, $q_x = 2\pi n z_1 / dz_2$, and $q_y \sim 0$. The spiral phase distribution for the $\pm n$ th diffraction from a grating with $b = 1$ can be extracted by filtering $G_n^\pm(q_x, q_y)$, followed by an inverse Fourier transform \mathcal{F}^{-1} and multiplying by the term e^{-ikR_2} , as follows:

$$I'_{\pm n} = e^{-ikR_2} \mathcal{F}^{-1}[G_n^\pm] \quad (15)$$

$$= -iC_n |\mathcal{J}'_n(\rho_{f, \pm n})| e^{i(\pm \ell \phi_{f, \pm n} + \alpha_{\pm n})}, \quad (16)$$

where the double signs are taken in the same order in each case. Figures 3(a) and 3(b) present the absolute values of I'_n for the Bragg diffractions obtained in our experiment, where the stripelike intensity modulation vanishes in both cases. The intensity patterns are similar to those for the Bragg diffractions with $\ell = \pm 1$ without interference, as shown in Fig. 1(d), in which a singularity appears at the center owing to the term $|\mathcal{J}'_n|$. Furthermore, we successfully obtain a spiral phase distribution for vortex beams with $\ell = -1$ and $\ell = +1$ with a single phase singularity

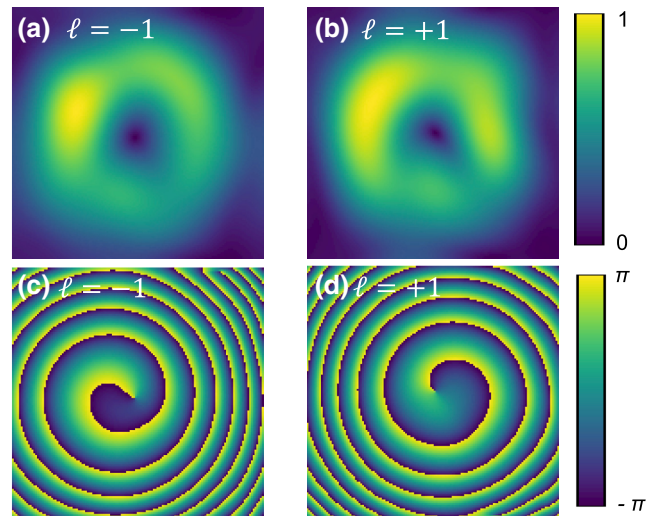


FIG. 3. (a),(b) Contours of the absolute value of I'_n obtained in the way described in the text for the Bragg diffractions with (a) $\ell = -1$ and (b) $\ell = +1$, which are shown in Fig. 2(a). (c),(d) Spiral phase distribution for vortex diffraction waves with (c) $\ell = -1$ and (d) $\ell = +1$.

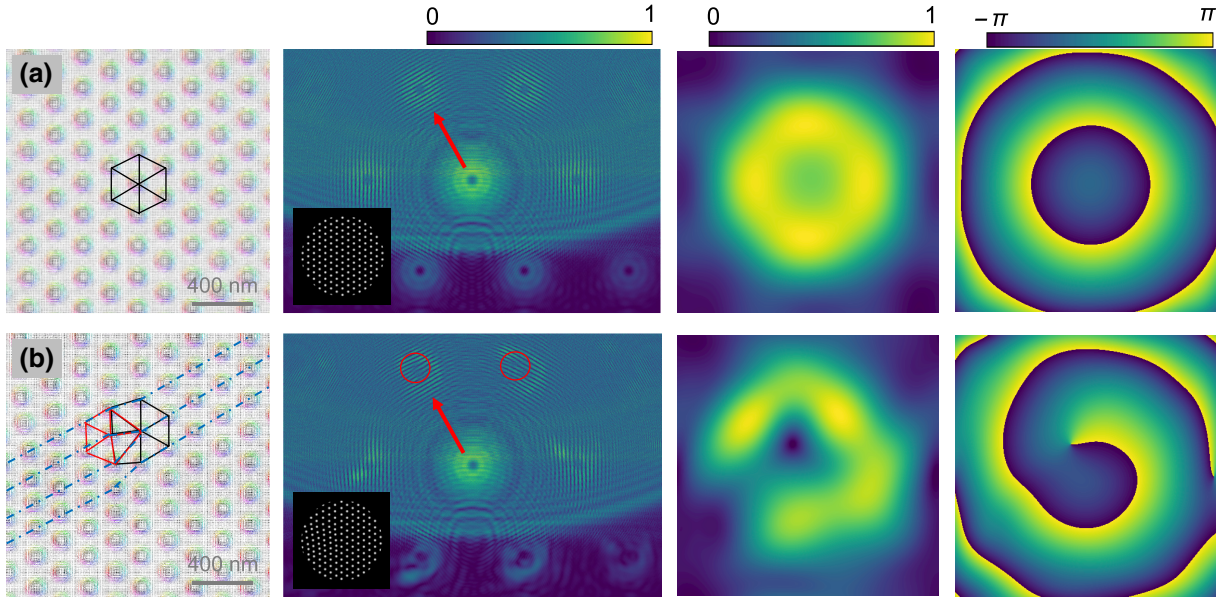


FIG. 4. Simulation of inline holography for a hexagonal SkL (a) and a SkL with a dislocation in the skyrmions (b). We calculate the corresponding interference diffraction patterns (second column), the absolute values of I'_n (third column), and the phase distribution (fourth column) of the diffracted waves, indicated by red arrows in the second column. The insets in the second column represent images of the z component of the magnetic moment in the corresponding SkLs. The images of SkLs shown in the first column are visualized using the Spirit framework [29].

by extracting the phase term from I'_n , as shown in Figs. 3(c) and 3(d), respectively, where the rotation direction is reversed between the $\ell = \pm 1$ diffracted waves. In addition, the phase modulation in the radial direction due to the term $e^{i\alpha \pm n}$ yields a pattern like a Fermat's spiral as observed, which originates from the use of a divergent light source. (We also simulate inline holography for a fork grating with $b = 2$, as presented in the Supplemental Material [28].)

IV. SIMULATION FOR A MAGNETIC SKYRMION LATTICE

In the next step, we demonstrate a simulation of a practical application of the present technique to a dislocation in a magnetic skyrmion lattice (SkL). Magnetic skyrmions are nanoscale noncollinear spin textures and are stabilized by competition between ferromagnetic exchange, Zeeman, and Dzyalohsinskii-Moriya interactions. Skyrmions usually form a hexagonal lattice, as shown in Fig. 4(a), while they show arrangements with five and seven neighbors at domain boundaries, as reported in Ref. [13] [see also Fig. 4(b)]. Such a dislocation results in a fork-shaped pattern. Figures 4(a) and 4(b) show a simulation of inline holography for a hexagonal SkL [part (a)] and a SkL with a dislocation [part (b)]. We assume circular-shaped samples as shown in the insets in the second column in Fig. 4, in which the SkLs are composed of skyrmions with a diameter of 200 nm. The simulated experimental geometry is same as that shown in Fig. 1(c). The samples are placed $z_1 = 600 \mu\text{m}$ away from the focal point, in the lower part

of the annular diffracted waves from the FZP. This geometry results in the interference diffraction patterns shown in the second column in Fig. 4. Both pattern show a sixfold intensity distribution reflecting the hexagonal symmetry of the SkL, while the diagonal diffraction from the zeroth-order diffraction point shows a fork-shaped pattern in the case of the SkL with a dislocation. These interference patterns indicate that an incident soft-x-ray beam can be converted to a vortex beam via a dislocation at a magnetic domain boundary in a SkL. The third and fourth columns in Fig. 4 show the absolute values of I'_n and the phase distributions for the diffracted waves indicated by the red arrows in the second column. In the case of a SkL with a dislocation, the diagonal diffracted wave shows a spiral phase distribution with a phase singularity, which reflects the topological features of a dislocation in a SkL.

V. SUMMARY

To summarize, we successfully observe the intensity and phase distributions of soft-x-ray vortex beams generated by a fork grating via inline holography. The present technique enables one to directly detect the spiral phase distribution of soft-x-ray vortices without any complicated analysis, and our results should make further progress in soft-x-ray methods possible. Furthermore, we demonstrate a simulation of an inline-holography experiment with a dislocation in a SkL, which implies that soft-x-ray inline holography may pave the way to characterization of topological defects in magnetic textures.

ACKNOWLEDGMENT

We thank M. Hatayama and J. Sasakura at NTT-AT for preparing the fork-shaped grating. This work was supported in part by PRESTO Grant No. JP-MJPR177A, by Grants-in-Aid for Scientific Research No. JP16H05990, No. JP17K05130, No. JP19H04399, No. JP19K23590, and No. JP20H04458, by MEXT Quantum Leap Flagship Program (MEXT Q-LEAP) Grant No. JPMXS0120184122, and by the Research Foundation for Opto-Science and Technology. The soft-x-ray scattering work was performed with the approval of the Photon Factory Program Advisory Committee (Proposals No. 2015S2-007, No. 2018S2-006, No. 2019G590, and No. 2019PF-22).

APPENDIX: EXTRACTION OF PHASE DISTRIBUTION OF DIFFRACTED WAVES BY INLINE HOLOGRAPHY

We suppose that there is a virtual point light source with an intensity u_0 and a wavelength λ located at the origin of Cartesian coordinates and that the light propagates along the z axis. From Huygens' principle [27], the light field u_2^d at a detector point $P = (x_2, y_2, z_2)$ can be written as

$$u_2^d(P) = \frac{u_0 e^{iks}}{s} \sim \frac{u_0 e^{ik[z_2 + (x_2^2 + y_2^2)/2z_2]}}{z_2}, \quad (\text{A1})$$

where $k = 2\pi/\lambda$ and $s = \sqrt{x_2^2 + y_2^2 + z_2^2}$, using the paraxial approximation. Here, we consider unpolarized soft x rays for simplicity. Supposing that a circular fork-shaped grating is located at (x_g, y_g) in the $z = z_1$ plane, we consider a light beam that passes through a position $Q = (x'_1, y'_1, z_1) = (x_g + x_1, y_g + y_1, z_1)$ on the grating, diffracts, and is finally observed at a point P . The light field at the point Q is

$$u_1(Q) = \frac{u_0 e^{ikt}}{t}, \quad (\text{A2})$$

where $t = \sqrt{(x_g + x_1)^2 + (y_g + y_1)^2 + z_1^2}$, and thus the diffracted light at the point P can be calculated from

$$u_2^g(P) = -\frac{i}{\lambda} \iint_S \frac{e^{ikr}}{r} a(Q) u_1(Q) dx_1 dy_1, \quad (\text{A3})$$

where S denotes the region of the grating over which the integral is taken, and $r = \sqrt{(x'_1 - x_2)^2 + (y'_1 - y_2)^2 + (z_1 - z_2)^2}$. $a(Q)$ indicates the binarized transmittance of the fork-shaped grating. Using the paraxial approximation, the light field can be

rewritten as

$$u_2^g(P) \sim -\frac{iu_0}{\lambda z_1 (z_2 - z_1)} \iint_S a(Q) e^{ik(t+r)} dx_1 dy_1, \quad (\text{A4})$$

and

$$\begin{aligned} t + r &\sim z_1 + \frac{x_1'^2 + y_1'^2}{2z_1} + (z_2 - z_1) \\ &\quad + \frac{(x_2 - x_1')^2 + (y_2 - y_1')^2}{2(z_2 - z_1)} \\ &= L_0 - \frac{(x_2 - x_g z_2/z_1)x_1 + (y_2 - y_g z_2/z_1)y_1}{z_2 - z_1} \\ &\quad + \frac{x_1^2 + y_1^2}{2(z_2 - z_1)z_1/z_2}, \end{aligned} \quad (\text{A5})$$

where L_0 consists of terms that are independent of x_1 and y_1 :

$$\begin{aligned} L_0 &= z_2 + \frac{x_2^2 + y_2^2}{2(z_2 - z_1)} + \frac{x_g^2 + y_g^2}{2(z_2 - z_1)z_1/z_2} \\ &\quad - \frac{x_g x_2 + y_g y_2}{(z_2 - z_1)}. \end{aligned} \quad (\text{A6})$$

This can be expressed as

$$\begin{aligned} u_2^g(P) &= -\frac{iu_0 e^{ikL_0}}{\lambda z_1 (z_2 - z_1)} \\ &\quad \times \iint_S a(Q) e^{-i(f'_x x_1 + f'_y y_1)} e^{if_0(x_1^2 + y_1^2)} dx_1 dy_1, \end{aligned} \quad (\text{A7})$$

where

$$f'_x = \frac{k}{z_2 - z_1} \left(x_2 - x_g \frac{z_2}{z_1} \right), \quad (\text{A8})$$

$$f'_y = \frac{k}{z_2 - z_1} \left(y_2 - y_g \frac{z_2}{z_1} \right), \quad (\text{A9})$$

$$f_0 = \frac{kz_2}{2z_1(z_2 - z_1)}, \quad (\text{A10})$$

which corresponds to near-field diffraction, i.e., Fresnel diffraction [27]. If the Fourier transform f is denoted by $\mathcal{F}[f]$, this can be simply rewritten as

$$u_2^g(P) = -\frac{iu_0 e^{ikL_0}}{\lambda z_1 (z_2 - z_1)} \mathcal{F}[a(Q) e^{if_0(x_1^2 + y_1^2)}]. \quad (\text{A11})$$

The diffraction pattern of these two waves is given by

$$\begin{aligned} I(P) &= |u_2^d(P) + u_2^g(P)|^2 \\ &= |u_2^d(P)|^2 + |u_2^g(P)|^2 + u_2^d(P) u_2^{g*}(P) + \text{c.c.} \end{aligned} \quad (\text{A12})$$

The third and fourth terms correspond to the interference term. Using the paraxial approximation, this can be written

as

$$I(P) = \frac{u_0^2}{z_2^2} + \left| \frac{u_0 \mathcal{F}[a(Q)e^{if_0(x_1^2+y_1^2)}]}{\lambda z_1(z_2 - z_1)} \right|^2 - 2 \operatorname{Re} \left[\frac{i u_0^2 e^{ikR_2}}{\lambda z_1 z_2 (z_2 - z_1)} \mathcal{F}[a(Q)e^{if_0(x_1^2+y_1^2)}] \right], \quad (\text{A13})$$

where

$$R_2 = L_0 - z_2 - \frac{x_2^2 + y_2^2}{2z_2} = \frac{z_1}{2z_2(z_2 - z_1)} \left\{ \left(x_2 - \frac{z_2}{z_1} x_g \right)^2 + \left(y_2 - \frac{z_2}{z_1} y_g \right)^2 \right\}, \quad (\text{A14})$$

which suggests that the interference scattering gives rise to concentric fringes centered on $(x_2, y_2) = [(z_2/z_1)x_g, (z_2/z_1)y_g]$.

Next, we consider the Fourier transform $\mathcal{F}[a(Q)e^{if_0(x_1^2+y_1^2)}]$. The phase distribution in a fork grating with a pitch d and a topological number b is expressed as in Eq. (2). The binarized amplitude is given by Eq. (3), and is written in the form of a Fourier series as [25]

$$a(\varphi) = \sum_{n=-\infty}^{\infty} \frac{\sin(n\pi/2)}{n\pi} e^{-in(\pi/2)} e^{in\varphi} \equiv \sum_{n=-\infty}^{\infty} A_n e^{-in(\pi/2)} e^{in\varphi}. \quad (\text{A15})$$

Changing the Fourier transform to one in cylindrical coordinates, this can be written as

$$\begin{aligned} \mathcal{F}[a(Q)e^{if_0(x_1^2+y_1^2)}] &= \mathcal{F}[a(\rho, \phi)e^{if_0\rho^2}] \\ &= \sum_{n=-\infty}^{\infty} A_n e^{-in(\pi/2)} \mathcal{F}[e^{inb\phi + in(2\pi/d)\rho \cos\phi + if_0\rho^2}] \\ &= \sum_{n=-\infty}^{\infty} A_n e^{-in(\pi/2)} \mathcal{F}[e^{inb\phi} e^{if_0\rho^2}] * \mathcal{F}[e^{in(2\pi/d)\rho \cos\phi}] \\ &= \sum_{n=-\infty}^{\infty} A_n e^{-in(\pi/2)} \mathcal{F}[e^{inb\phi} e^{if_0\rho^2}] * \delta\left(f_x' - \frac{2n\pi}{d}\right), \end{aligned} \quad (\text{A16})$$

where $*$ is the convolution integral and δ is the delta function. Using cylindrical coordinates in the Fourier space

$$(\rho_f, \phi_f) = \left(\sqrt{f_x'^2 + f_y'^2}, \operatorname{atan}(f_y'/f_x') \right),$$

$$\begin{aligned} \mathcal{F}[e^{inb\phi} e^{if_0\rho^2}] &= \int_0^a \int_0^{2\pi} e^{inb\phi} e^{if_0\rho^2} e^{i\rho_f \rho \cos(\phi - \phi_f)} \rho d\rho d\phi \\ &= \int_0^a \int_0^{2\pi} e^{if_0\rho^2} e^{inb\phi_f} e^{i\rho_f \rho \cos\phi' + inb\phi'} \rho d\rho d\phi' \\ &= 2\pi e^{inb(\phi_f + \pi/2)} \int_0^a e^{if_0\rho^2} \rho J_{nb}(\rho_f \rho) d\rho, \end{aligned} \quad (\text{A17})$$

where

$$J_n(z) = \frac{i^{-n}}{2\pi} \int_0^{2\pi} e^{iz \cos\phi + in\phi} d\phi \quad (\text{A18})$$

is the Bessel function of the first kind, and the radius of the grating is a . Then the Fourier transform finally becomes

$$\begin{aligned} \mathcal{F}[a(Q)e^{if_0(x_1^2+y_1^2)}] &= \sum_{n=-\infty}^{\infty} 2\pi A_n |\mathcal{J}'_{nb}(\rho_{fn})| e^{-in\pi/2} e^{inb(\phi_{fn} + \pi/2)} e^{i\alpha_{nb}(\rho_{fn})}, \end{aligned} \quad (\text{A19})$$

where

$$\mathcal{J}'_{nb}(\rho_f) \equiv \int_0^a e^{if_0\rho^2} \rho J_{nb}(\rho_f \rho) d\rho = |\mathcal{J}'_{nb}(\rho_f)| e^{i\alpha_{nb}(\rho_f)}, \quad (\text{A20})$$

and where (ρ_{fn}, ϕ_{fn}) are cylindrical coordinates with origin $(f_x, f_y) = (2n\pi/d, 0)$. Equation (A19) indicates that the n th Bragg-diffracted wave has a so-called topological charge $\ell = nb$, which is defined as the azimuthal mode index of a Laguerre-Gaussian mode [1]. If the different orders of the grating diffractions are sufficiently far apart, the intensity can be written as

$$\begin{aligned} I(P) &= \frac{u_0^2}{z_2^2} + \sum_{n=-\infty}^{\infty} \left(\frac{2\pi u_0 A_n |\mathcal{J}'_{nb}(\rho_{fn})|}{\lambda z_1 (z_2 - z_1)} \right)^2 \\ &\quad + 4\pi \sum_{n=-\infty}^{\infty} \frac{u_0^2 A_n |\mathcal{J}'_{nb}(\rho_{fn})|}{\lambda z_1 z_2 (z_2 - z_1)} \\ &\quad \times \sin \left\{ kR_2 + nb\phi_{fn} + n(b-1)\frac{\pi}{2} + \alpha_{nb}(\rho_{fn}) \right\}. \end{aligned} \quad (\text{A21})$$

For the n th-order diffraction from a $b = 1$ grating, the angle θ in the sine function in Eq. (A21) can be written as

$$\theta_n = kR_2 + n\phi_{fn} + \alpha_n = B(f_x'^2 + f_y'^2) + n\phi_{fn} + \alpha_n, \quad (\text{A22})$$

where $B = z_1(z_2 - z_1)/2z_2k$. Around the n th diffraction, this can be written as

$$\begin{aligned}\theta_n &= B \left(f'_x - \frac{2n\pi}{d} \right)^2 + \frac{4n\pi}{d} B f'_x + B f_y'^2 \\ &\quad - B \left(\frac{2n\pi}{d} \right)^2 + n\phi_{f_n} + \alpha_n \\ &= B \rho_{f_n}^2 + \frac{4n\pi}{d} B f'_x - B \left(\frac{2n\pi}{d} \right)^2 + n\phi_{f_n} + \alpha_n.\end{aligned}\quad (\text{A23})$$

The n th Bragg diffraction can be expressed as

$$\begin{aligned}I_n(P) &= \frac{u_0^2}{z_2^2} + \left(\frac{2\pi u_0 A_n |\mathcal{J}'_{nb}(\rho_{f_n})|}{\lambda z_1 (z_2 - z_1)} \right)^2 \\ &\quad + 2\pi \frac{u_0^2 A_n |\mathcal{J}'_{nb}(\rho_{f_n})|}{i\lambda z_1 z_2 (z_2 - z_1)} (e^{i\theta_n} - e^{-i\theta_n}).\end{aligned}\quad (\text{A24})$$

Since the Fourier transform of $De^{i\theta_n}$ into the Fourier space (μ, ν) can be expressed as

$$\begin{aligned}\mathcal{F}[De^{i\theta_n}] &\equiv \iint De^{i\theta} e^{-i(\mu f'_x + \nu f'_y)} df'_x df'_y \\ &= \mathcal{F}[De^{i[\theta_n - (4n\pi/d)Bf'_x]}] * \mathcal{F}[e^{i(4n\pi/d)Bf'_x}] \\ &= \mathcal{F}[De^{i[\theta_n - (4n\pi/d)Bf'_x]}] * \delta\left(\mu - \frac{4n\pi}{d}B\right),\end{aligned}\quad (\text{A25})$$

the Fourier transform $\mathcal{F}(I_n)$ gives rise to peaks around $\mu = 0, \pm 4n\pi B/d$. Thus $\mathcal{F}(I_n)$ can be divided into three parts as below:

$$\mathcal{F}(I_n) = G_n^0(0, 0) + G_n^+(\mu_+, 0) + G_n^-(\mu_-, 0), \quad (\text{A26})$$

where $G_n^0(0, 0)$ represents the dc component of I_n and can be expressed as

$$G_n^0(0, 0) = \frac{u_0^2}{z_2^2} + \left(\frac{2\pi u_0 A_n |\mathcal{J}'_{nb}(\rho_{f_n})|}{\lambda z_1 (z_2 - z_1)} \right)^2, \quad (\text{A27})$$

and $G_n^\pm(\mu_\pm, 0)$ represents the ac component,

$$G_n^\pm(\mu_\pm, 0) = \mathcal{F} \left[2\pi \frac{u_0^2 A_n |\mathcal{J}'_{nb}(\rho_{f_n})|}{i\lambda z_1 z_2 (z_2 - z_1)} e^{\pm i\theta_n} \right], \quad (\text{A28})$$

with $\mu_\pm = \pm 4n\pi B/d$. Equation (A25) also means that the average stripe pitch around the n th ($n \neq 0$) diffraction can be obtained as

$$d' = \frac{1}{2|n|B} \frac{z_2 - z_1}{k} d = \frac{z_2}{|n|z_1} d. \quad (\text{A29})$$

The inverse Fourier transform of a filtered Fourier transform $\mathcal{F}[I_n(P)]$ around $\mu = 4n\pi B/d$ can be expressed

as

$$\mathcal{F}^{-1}[G_n^+] = 2\pi \frac{u_0^2 A_n |\mathcal{J}'_{nb}(\rho_{f_n})|}{i\lambda z_1 z_2 (z_2 - z_1)} e^{i(kR_2 + n\phi_{f_n} + \alpha_n)}. \quad (\text{A30})$$

Thus I'_n in Eq. (16) can be obtained as

$$\begin{aligned}I'_n(P) &= e^{-ikR_2} \mathcal{F}^{-1}[G_n^+] \\ &= 2\pi \frac{u_0^2 A_n |\mathcal{J}'_{nb}(\rho_{f_n})|}{i\lambda z_1 z_2 (z_2 - z_1)} e^{i(n\phi_{f_n} + \alpha_n)},\end{aligned}\quad (\text{A31})$$

which suggests that one can extract the phase distribution in the azimuthal direction superimposed on that in the radial direction originating from the Fresnel integral of the Bessel function.

- [1] L. Allen, M. W. Beijersbergen, R. J. C. Spreeuw, and J. P. Woerdman, Orbital angular momentum of light and the transformation of Laguerre-Gaussian laser modes, *Phys. Rev. A* **45**, 8185 (1992).
- [2] Y. Shen, X. Wang, Z. Xie, C. Min, X. Fu, Q. Liu, M. Gong, and X. Yuan, Optical vortices 30 years on: OAM manipulation from topological charge to multiple singularities, *Light: Sci. Appl.* **8**, 1 (2019).
- [3] Q. Xiaodong, L. FanGshu, Z. Wuhong, Z. Zhihan, and C. Lixiang, Spiral phase contrast imaging in nonlinear optics: Seeing phase objects using invisible illumination, *Opt. Soc. Am.* **5**, 208 (2018).
- [4] David G. Grier, A revolution in optical manipulation, *Nature* **424**, 810 (2003).
- [5] M.-T. Gabriel, P. T. Juan, and T. Lluis, Twisted photons, *Nat. Phys.* **3**, 305 (2007).
- [6] J. Bahrtdt, K. Holldack, P. Kuske, R. Müller, M. Scheer, and P. Schmid, First Observation of Photons Carrying Orbital Angular Momentum in Undulator Radiation, *Phys. Rev. Lett.* **111**, 034801 (2013).
- [7] A. Sakdinawat and Y. Liu, Soft-x-ray microscopy using spiral zone plates, *Opt. Lett.* **32**, 2635 (2007).
- [8] J. C. T. Lee, S. J. Alexander, S. D. Kevan, S. Roy, and B. J. McMorran, Laguerre-Gauss and Hermite-Gauss soft X-ray states generated using diffractive optics, *Nat. Photonics* **13**, 205 (2019).
- [9] Y. Yamasaki, D. Morikawa, T. Honda, H. Nakao, Y. Murakami, N. Kanazawa, M. Kawasaki, T. Arima, and Y. Tokura, Dynamical process of skyrmion-helical magnetic transformation of the chiral-lattice magnet FeGe probed by small-angle resonant soft x-ray scattering, *Phys. Rev. B* **92**, 220421 (2015).
- [10] V. Ukleev, Y. Yamasaki, D. Morikawa, N. Kanazawa, Y. Okamura, H. Nakao, Y. Tokura, and T. Arima, Coherent resonant soft x-ray scattering study of magnetic textures in fege, *Quantum Beam Sci.* **2**, 3 (2018).
- [11] V. Ukleev, Y. Yamasaki, D. Morikawa, K. Karube, K. Shibata, Y. Tokunaga, Y. Okamura, K. Amemiya, M. Valvidares, H. Nakao, Y. Taguchi, Y. Tokura, and T. Arima, Element-specific soft x-ray spectroscopy, scattering, and

- imaging studies of the skyrmion-hosting compound $\text{Co}_8\text{Zn}_8\text{Mn}_4$, *Phys. Rev. B* **99**, 144408 (2019).
- [12] Y. Takahashi, A. Suzuki, S. Furutaku, K. Yamauchi, Y. Kohmura, and T. Ishikawa, Bragg x-ray ptychography of a silicon crystal: Visualization of the dislocation strain field and the production of a vortex beam, *Phys. Rev. B* **87**, 121201 (2013).
- [13] J. Rajeswari, P. Huang, G. F. Mancini, Y. Murooka, T. Latychevskaya, D. McGrouther, M. Cantoni, E. Baldini, J. S. White, A. Magrez, T. Giamarchi, H. M. Rønnow, and F. Carbone, Filming the formation and fluctuation of skyrmion domains by cryo-lorentz transmission electron microscopy, *Proc. Natl. Acad. Sci.* **112**, 14212 (2015).
- [14] H. Nakajima, A. Kotani, M. Mochizuki, K. Harada, and S. Mori, Formation process of skyrmion lattice domain boundaries: The role of grain boundaries, *Appl. Phys. Lett.* **111**, 192401 (2017).
- [15] F. Zheng, F. N. Rybakov, A. B. Borisov, D. Song, S. Wang, Z.-A. Li, H. Du, N. S. Kiselev, J. Caron, A. Kovács, M. Tian, Y. Zhang, S. Blügel, and R. E. Dunin-Borkowski, Experimental observation of chiral magnetic bobbars in B20-type FeGe, *Nat. Nanotechnol.* **13**, 451 (2018).
- [16] M. T. Birch *et al.*, Real-space imaging of confined magnetic skyrmion tubes, *Nat. Commun.* **11**, 1726 (2020).
- [17] M. Harris, C. A. Hill, P. R. Tapster, and J. M. Vaughan, Laser modes with helical wave fronts, *Phys. Rev. A* **49**, 3119 (1994).
- [18] Z. Wang, Z. Zhang, and Q. Lin, A novel method to determine the helical phase structure of Laguerre–Gaussian beams, *J. Opt. A: Pure Appl. Opt.* **11**, 085702 (2009).
- [19] K. Saitoh, Y. Hasegawa, K. Hirakawa, N. Tanaka, and M. Uchida, Measuring the Orbital Angular Momentum of Electron Vortex Beams Using a Forked Grating, *Phys. Rev. Lett.* **111**, 074801 (2013).
- [20] K. Harada, K. Shimada, and Y. A. Ono, Electron holography for vortex beams, *Appl. Phys. Express* **13**, 032003 (2020).
- [21] M. W. Beijersbergen, L. Allen, H. E. L. O. van der Veen, and J. P. Woerdman, Astigmatic laser mode converters and transfer of orbital angular momentum, *Opt. Commun.* **96**, 123 (1993).
- [22] V. Bazhenov, M. Vasnetsov, and M. Soskin, Laser beams with screw dislocations in their wavefronts, *JETP Lett.* **52**, 429 (1990).
- [23] J. Arlt, K. Dholakia, L. Allen, and M. J. Padgett, The production of multiringed Laguerre–Gaussian modes by computer-generated holograms, *J. Mod. Opt.* **45**, 1231 (1998).
- [24] A. Dussaux, P. Schoenherr, K. Koumpouras, J. Chico, K. Chang, L. Lorenzelli, N. Kanazawa, Y. Tokura, M. Garst, A. Bergman, C. L. Degen, and D. Meier, Local dynamics of topological magnetic defects in the itinerant helimagnet FeGe, *Nat. Commun.* **7**, 12430 (2016).
- [25] G. Zhang, M. Zhang, and Y. Zhao, Wave front control with SLM and simulation of light wave diffraction, *Opt. Express* **26**, 33543 (2018).
- [26] D. H. Bailey and P. N. Swartztrauber, The fractional Fourier transform and applications, *Soc. Ind. Appl. Math.* **33**, 389 (1991).
- [27] B. Max and W. Emil, *Principles of Optics* (Pergamon, New York, 1970).
- [28] See Supplemental Material at <http://link.aps.org/supplemental/10.1103/PhysRevApplied.14.064069> for simulation of inline holography for a fork grating with $b = 2$.
- [29] G. P. Müller, M. Hoffmann, C. Dißelkamp, D. Schürhoff, S. Mavros, M. Sallermann, N. S. Kiselev, H. Jónsson, and S. Blügel, Spirit: Multifunctional framework for atomistic spin simulations, *Phys. Rev. B* **99**, 224414 (2019).